

Manuscript Number: CEMCON-D-11-00691R1

Title: Rietveld quantitative phase analysis of Yeelimite-containing cements

Article Type: Research Paper

Keywords: $4\text{CaO}\cdot 3\text{Al}_2\text{O}_3\cdot \text{CaSO}_4$
Sulfoaluminate
X-Ray Diffraction
Amorphous Material
Characterization

Corresponding Author: Dr MIGUEL A. G. ARANDA, PhD

Corresponding Author's Institution: Universidad de Málaga

First Author: Gema Álvarez-Pinazo

Order of Authors: Gema Álvarez-Pinazo; Ana Cuesta; Marta García-Maté; Isabel Santacruz; Enrique R Losilla; Angeles G De la Torre; Laura León-Reina; MIGUEL A. G. ARANDA, PhD

Abstract: Yeelimite-containing cements are attracting attention for their tailored properties. Calcium sulfoaluminate, CSA, cements have high contents of Yeelimite and they are used for special applications. Belite calcium sulfoaluminate, BCSA or sulfobelite, cements have high contents of belite and intermediate contents of Yeelimite, and they may become an alternative to OPC. Here, we report Rietveld quantitative phase analyses for three commercially available CSA clinkers, one CSA cement, and two laboratory-prepared iron-rich BCSA clinkers. The crystalline phases are reported and quantified. Selective dissolutions are employed for BCSA clinkers to firmly establish their phases. Finally, the overall unaccounted contents (amorphous plus crystalline not quantified) have been determined by two approaches: i) external standard procedure (G-method) with reflection data; ii) internal standard procedure (spiking method with ZnO) with transmission data. The overall unaccounted contents for CSA clinkers were ~10 wt%. Conversely, the unaccounted contents for BCSA clinkers were higher, ~25 wt%.

1 [Revised manuscript \(CEMCON-D-11-00691\)](#) submitted to *Cement and Concrete Research*

2 **Rietveld quantitative phase analysis of Yeelimate-containing cements**

3 G. Álvarez-Pinazo¹, A. Cuesta¹, M. García-Maté¹, I. Santacruz¹, E. R. Losilla,¹ A. G. De la Torre¹,
4 L. León-Reina² and M. A. G. Aranda^{*1}

5 ¹ Departamento de Química Inorgánica, Cristalografía y Mineralogía, Universidad de Málaga,
6 29071 Málaga, Spain

7 ² Servicios Centrales de Apoyo a la Investigación, Universidad de Málaga, 29071-Málaga, Spain

8 **Abstract.**

9 Yeelimate-containing cements are attracting attention for their tailored properties. Calcium
10 sulfoaluminate, CSA, cements have high contents of Yeelimate and they are used for special
11 applications. Belite calcium sulfoaluminate, BCSA or sulfobelite, cements have high contents of
12 belite and intermediate contents of Yeelimate, and they may become an alternative to OPC. Here,
13 we report Rietveld quantitative phase analyses for three commercially available CSA clinkers, one
14 CSA cement, and two laboratory-prepared iron-rich BCSA clinkers. The crystalline phases are
15 reported and quantified. Selective dissolutions are employed for BCSA clinkers to firmly establish
16 their phases. Finally, the overall unaccounted contents (amorphous plus crystalline not quantified)
17 have been determined by two approaches: i) external standard procedure (G-method) with reflection
18 data; ii) internal standard procedure (spiking method with ZnO) with transmission data. The overall
19 unaccounted contents for CSA clinkers were ~10 wt%. Conversely, the unaccounted contents for
20 BCSA clinkers were higher, ~25 wt%.

21 **Keywords:** $4\text{CaO}\cdot 3\text{Al}_2\text{O}_3\cdot \text{CaSO}_4$; calcium sulfoaluminate; X-Ray Diffraction analysis; Rietveld
22 method; amorphous material

23 *Corresponding author. Tel.: +34952131874; fax: +34952132000; *E-mail address:*
24 g_aranda@uma.es (Miguel A. G. Aranda)

25 **1. Introduction.**

26 Calcium sulfoaluminate (CSA) cements have been applied worldwide from the 60's as expansive
27 binders mixed with Portland cements [1]. These cements are characterised by containing high
28 amounts of Yeelimite, also called Klein's salt or tetracalcium trialuminate sulfate ($C_4A_3\underline{S}$).
29 Hereafter, cement nomenclature will be used, i.e. C=CaO, S=SiO₂, A=Al₂O₃, F=Fe₂O₃, M=MgO,
30 \underline{S} =SO₃, \underline{C} =CO₂, H=H₂O, K=K₂O and N=Na₂O. Therefore, $C_4A_3\underline{S}$ corresponds to Ca₄Al₆O₁₂(SO₄).
31 During the 70's, CSA cements were introduced into the Chinese market as high performance and
32 dimensionally stable cementitious matrices developed by China Building Materials Academy [2]. In
33 Europe, the use of CSA cements is strongly limited by the lack of standards concerning special
34 cements derived from non-Portland clinkers. Nevertheless, their manufacture has recently been
35 started by several companies. The main uses of these CSA cements, or blends with Portland
36 cements, are for quick repairs and pre-cast products or floor concrete applications.

37 Moreover, Yeelimite-containing cements have become highly popular over the last few years for
38 research. The driving force for these investigations is much lower CO₂ emissions in their
39 manufacture when compared to those of Portland cement production due to the following main
40 reasons [3,4]: i) Yeelimite releases during its synthesis only a third part of the CO₂ released by the
41 production of alite, ii) firing temperature is about 200°C lower than that of OPC clinker, iii) various
42 industrial by-products can be used in the kiln feed, and iv) Yeelimite-containing clinkers are easier
43 to grind than OPC clinkers. The improvement of cement performances and the reduction of the
44 environmental impact related to its manufacture are most likely the main areas of innovation for the
45 cement industry [5]. It must be highlighted that CSA cements may have important special
46 applications such radioactive element encapsulation in high-density cement pastes [6]. Other
47 interesting properties of Yeelimite-containing cements are high early strengths, short setting times,

48 low solution alkalinity as well as high impermeability and chemical resistance against several
49 aggressive media [7].

50 However, while the composition of Portland cement is defined by long-standing codes and
51 standards, there is no corresponding compositional framework for Yeelimite-containing cements.
52 These clinkers may show very variable phase assemblage. The raw mix composition can be based
53 on conventional raw materials (limestone, clay, bauxite and iron ores); in addition, industrial by-
54 products and wastes can also be added [8,9]. Yeelimite-containing cements could be classified
55 according to their C_4A_3S contents as:

56 I) Calcium Sulfo-Aluminate (CSA) cements which would refer to those with high C_4A_3S
57 contents. They may be prepared from CSA clinkers containing C_4A_3S as the main phase ranging
58 between 50 to 90 wt% [10]. The calcium sulfate addition is very important as it may profoundly
59 affect the properties of the resulting binder [11-13]. The calcium sulfate source and content have
60 to be customized for a given application. These cements can be used alone or in combination
61 with other cements to provide an improved early resistance, low shrinkage, high
62 impermeability, and a strong resistance to sulfate attack.

63 II) Belite Calcium Sulfo-Aluminate (BCSA) cements which would refer to those with C_2S
64 (belite) as the main phase and intermediate C_4A_3S contents. These cements, also known as
65 sulfobelite, are prepared from clinkers containing more than 40-50 wt% of C_2S and 20-30%
66 C_4A_3S . The most common formulation of BCSA clinkers consists on β - C_2S , C_4A_3S and C_4AF
67 [6, 14-18]. These are iron-rich BCSA cements, also termed as BCSAF, and they are produced at
68 $\sim 1250^\circ\text{C}$ and show a rapid hardening, excellent durability, self-stressing and volume stability,
69 depending on the amount of gypsum added [19]. Recently, a new class of BCSAF cement has
70 been proposed by Lafarge [15,20,21] in which stabilization of high temperature belite

71 polymorphs (α -forms) has been promoted (for instance with borax) to enhance early age
72 hydration of these cements.

73 Alternatively, in order to further enhance mechanical strengths at very early ages, <1 day, C_4AF
74 phase may be substituted by $C_{12}A_7$; however, the clinkering temperature should be increased
75 $\sim 100^\circ\text{C}$ and the durability with respect to sulfate attack is limited [22,23]. This formulation
76 corresponds to aluminium-rich BCSA clinkers (or BCSAA) with C_2S , C_4A_3S , $C_{12}A_7$ and CA as
77 main phases [24]. In this type of clinkers, aluminate phases and C_4A_3S are responsible for the
78 early strength development, while C_2S provides hardening at much later ages. An in-situ study
79 of the clinkering of both BCSAF and BCSAA samples has been very recently reported using
80 high-energy synchrotron X-ray powder diffraction [25].

81 III) Alite Calcium Sulfo-Aluminate (ACSA) cements which would correspond to those
82 characterized by the simultaneous presence of C_3S and C_4A_3S phases. In this special case,
83 Yeelite phase content may be even higher than that of alite [26]. Other phases may appear in
84 the clinkers including C_2S and C_3A . However, this type of clinker is quite difficult to prepare
85 because the optimum temperatures for the synthesis of the two phases differ considerably.
86 Nevertheless the addition of a small amount of CaF_2 (and/or CuO , TiO_2) to the raw mixes
87 allows the coexistence of both phases at temperatures between 1230 and 1300°C .

88 CSA and BCSA clinkers are complex materials due to the presence of many crystalline phases,
89 some of them also displaying polymorphism. X-ray powder diffraction (XRPD) is the most
90 appropriate technique to identify, characterize and quantify the crystalline phases within these
91 samples. The application of Rietveld methodology [27] to XRPD data in order to obtain quantitative
92 phase analyses (RQPA) was reported long time ago [28]. To derive the phase contents from the
93 Rietveld optimised scale factors, this methodology normalizes the results to 100% of crystalline
94 phases (*i.e.* the presence of amorphous content is not taken into account). Therefore, if the mixture

95 has an appreciable amount of amorphous phase, this method is considered as semi-quantitative. To
96 overcome this problem, two approaches have been developed, the internal and the external standard
97 methods (to be briefly described just below). The presence of a glassy or amorphous component in
98 Portland cements and clinkers has been debated by several authors [29-31].

99 I) Internal standard method or “spiking method”, which consists on the addition of a known
100 amount of a crystalline standard, W_{st} . This standard must be free of amorphous content or at
101 least it should contain a known non-diffracting content. This (artificial) mixture must be well
102 homogenised since the particles should be randomly arranged. The addition of the standard will
103 dilute the crystalline phases within the samples, hence this may be a problem for low-content
104 phases. A procedure for Rietveld quantitative amorphous content analysis was outlined
105 elsewhere [32] and the effects of systematic errors in the powder patterns were studied. A very
106 recent report uses this methodology in depth [33]. This method permits the determination of an
107 overall unaccounted content which is composed by amorphous phase(s), misfitting problems of
108 the analysed crystalline phases, and because some crystalline phases may not be included in the
109 control file due to several reasons (its crystal structure is not known, the phase was not
110 identified, etc.). This overall content is hereinafter named ACn which stands for Amorphous and
111 Crystalline not-quantified, to highlight that not only an amorphous fraction but any not-
112 computed crystalline phase and any misfit problem (for instance the lack of an adequate
113 structural description for a given phase) may contribute to this number.

114 II) External standard method (G-factor approach), which consists in recording two patterns (one
115 for the sample and another for the standard). It is possible to use an external standard method to
116 avoid the complications that may arise from mixing an internal standard with the sample. This
117 approach requires the recording of two patterns in identical diffractometer
118 configuration/conditions for Bragg-Brentano $\theta/2\theta$ reflection geometry. The method was

119 proposed by O'Connor and Raven [34] and very recently applied to anhydrous cements [35] and
120 to pastes [36]. This methodology is also known as G-method since the standard allows
121 calculating the G-factor of the diffractometer in the operating conditions. This calculated G-
122 factor represents a calibration factor for the whole experimental setup and comprises the used
123 diffractometer, radiation, optics, and all data acquisition conditions (f.i. detector configuration,
124 integration time, etc.). It is experimentally more demanding but it may have the brightest future
125 as it does not interfere with the hydration reactions.

126 In this work, we report Rietveld quantitative phase analysis for several Yeelimite-containing
127 clinkers and cements. Both CSA and BCSAF clinkers have been studied to illustrate the suitability
128 of Rietveld methodology. Furthermore, the ACn contents have been determined using both
129 strategies, internal and external standard procedures. The obtained results are discussed.

130 **2. Experimental section.**

131 **2.1. Material description.**

132 In this work, six different types of Yeelimite-containing samples have been investigated. Three of
133 them are commercially available CSA clinkers. A CSA cement prepared in an industrial trial, but
134 not commercially available, has been also studied. Finally, two BCSAF clinkers prepared in our
135 laboratory have been also analysed.

136 **2.1.1. Commercial CSA clinkers.**

137 The following commercial clinkers with high C_4A_3S contents (ranging between 55 to 70 wt%) have
138 been studied:

139 - ALIPRE® (2009), a CSA clinker industrially produced by Italcementi Group.

140 - BELITH_CS10, a CSA clinker industrially produced in China and marketed in Europe by Belith
141 (Belgium).

142 - S.A.cement, a CSA clinker industrially produced by Buzzi Unicem.

143 **2.1.2. Non-commercial CSA cement.**

144 It has also been studied a CSA cement, with ~ 40% C_4A_3S , produced in an industrial trial which is
145 not commercially available. This cement is named CSA_trial in this study.

146 **2.1.3. Laboratory-prepared BCSAF clinkers.**

147 Approximately two kilograms of two BCSAF clinkers have been prepared in our laboratory in
148 several steps. The raw materials were weighed to have an expected phase composition of 50 wt%
149 C_2S , 30 wt% of C_4A_3S and 20 wt% of C_4AF . Table 1 shows the amounts of raw materials used for
150 the preparations. The difference in both samples is the addition of borax in one of them, 2 wt%
151 expressed as B_2O_3 in the resulting clinker. Hereafter, these clinkers are named BCSAF_B0 and
152 BCSAF_B2, for boron-free and boron-containing clinker, respectively. The raw materials mixture
153 (approximately 3 kilograms) was pre-homogenised for 15 minutes in a micro-Deval machine
154 (A0655, Proeti S.A., Spain) at 100 rpm with steel balls (9 balls of 30 mm, 21 balls of 18 mm and a
155 number of balls of 10 mm up to a total ball weight of 2500 g). The mixture was pressed into pellets
156 of about 40 g (55 mm of diameter and approximately 5 mm of height). Six pellets, one on top of
157 each other, were placed in a large Pt/Rh crucible of 325 ml of volume. The pellets were heated at
158 900°C and held for 30 min (heating rate of 5 °C/min). Then, they were further heated at 1350°C and
159 held for another 30 min (heating rate of 5 °C/min). Finally, the samples were quenched with air
160 flow. The clinkered pellets were grinded in the micro-Deval mill at 100 rpm for 1 hour. Under these
161 milling conditions, all clinker material passed through a 250 µm sieve.

162 **2.1.4. Selective dissolution of laboratory-prepared BCSAF clinkers.**

163 Selective dissolutions have been performed to study the laboratory-prepared BCSAF clinkers [37].

164 Initially, these clinkers were [ground](#) to a Blaine fineness of ~ 400 m²/kg.

165 **Selective dissolution to remove the aluminate phases (silicate residue).** A solution composed of
166 60 ml demineralised water, 8 g of KOH and 8 g of sucrose was heated to 95 °C with magnetic
167 stirring in a 250 ml beaker. After around 30 minutes, it becomes brown-yellow. Then, 4 g of clinker
168 powder was added and kept under stirring for 15 minutes. After this treatment, the resulting
169 suspension was filtered with a Whatman system (Whatman filter with diameter 70 mm). Once this
170 initial filtration step was finished, the minimum amount of water was added to eliminate the sucrose
171 and finally the residue was rinsed twice with isopropyl alcohol to remove water. After filtration, the
172 residue was mashed with a spatula to break up agglomerated particles, dried and analyzed by
173 XRPD.

174 **Selective dissolution to remove the silicate phases (aluminate residue).** A mixture of 4 g of
175 clinker powder, 52 ml methanol and 24 g salicylic acid was prepared. This mixture was stirred in a
176 250 ml beaker with a glass cover for 50 minutes. After that treatment, the mixture was filtered with
177 a Whatman system (Whatman filter with diameter 70 mm) and rinsed with ethanol. The residue was
178 dried in an oven at 60°C for 30 minutes, [ground](#) and analyzed by XRPD.

179 **2.2. Analytical techniques.**

180 **2.2.1. Elemental analysis by X-ray fluorescence.**

181 Table 2 gives the elemental analysis for the 6 studied samples [prepared as fused beads. The X-ray](#)
182 [fluorescence \(XRF\) data were taken](#) in a Magic X spectrometer (PANalytical, Almelo, The
183 Netherlands) using the calibration curve of silica-alumina materials. The elemental analyses of the
184 raw materials used for the BCSAF clinker preparations are available upon request, but they are not
185 reported here since the analyses of the clinkers are provided.

186 **2.2.2. Inductively coupled plasma mass spectroscopy (ICP-MS).**

187 The amounts of Na₂O and B₂O₃ in the laboratory-prepared BC SAF clinkers were determined by
188 ICP-MS on Perkin Elmer spectrophotometer (Nexion 300D). Previously, the samples were digested
189 in an Anton Paar device (Multiwave 3000) by using HNO₃, HCl and HF.

190 2.2.3. Laboratory X-ray powder diffraction.

191 All six samples were studied by laboratory X-ray powder diffraction (LXRPD) to identify,
192 characterize and quantify the crystalline phases. In order to study the ACn contents, both internal
193 and external standard approaches were employed.

194 On the one hand, the patterns studied by the **external standard** method were recorded in Bragg-
195 Brentano reflection geometry ($\theta/2\theta$) on an X'Pert MPD PRO diffractometer (PANalytical B.V.)
196 using strictly monochromatic CuK α_1 radiation ($\lambda=1.54059\text{\AA}$) [Ge (111) primary monochromator].
197 In addition to the patterns for the samples to be studied, this approach requires the recording of
198 additional patterns collected in identical diffractometer configuration/conditions for the standard, in
199 this case α -Al₂O₃ (SRM-676a). The X-ray tube worked at 45 kV and 40 mA. The optics
200 configuration was a fixed divergence slit ($1/2^\circ$), a fixed incident antiscatter slit (1°), a fixed
201 diffracted anti-scatter slit ($1/2^\circ$) and X'Celerator RTMS (Real Time Multiple Strip) detector,
202 working in scanning mode with maximum active length. Data were collected from 5° to 70° (2θ) for
203 ~ 2 hours. The samples were rotated during data collection at 16 rpm in order to enhance particle
204 statistics. NIST standard reference material SRM-676a, corundum (α -Al₂O₃) powder, has been
205 certified to have a crystalline phase purity of $99.02\% \pm 1.11\%$ (95% confidence interval) by RQPA
206 against a suitable primary standard, powder silicon carefully prepared from a single crystal [33].

207 On the other hand, the patterns studied by the **internal standard** method were recorded in flat-
208 sample transmission geometry on an EMPYREAN diffractometer (PANalytical B.V.) equipped
209 with a θ/θ goniometer, CuK $\alpha_{1,2}$ radiation ($\lambda=1.542\text{\AA}$) and a focusing mirror. This PreFIX optical

210 component is capable of converting the divergent beam into a convergent radiation focused on the
211 goniometer circle. The EMPYREAN diffractometer was equipped with fixed incident and diffracted
212 beam anti-scatter slits of $\frac{1}{4}^\circ$ and 5 mm, respectively. The detector was PIXCEL 3D RTMS, which
213 comprises more than 65000 pixels, each 55×55 microns in size; each having its own circuitry. As
214 internal standard, ZnO (99.99%, Sigma-Aldrich, St. Louis, MO, USA), was added to the samples to
215 a total content of 25 wt%. The mixtures were homogenized for 20 minutes in an agate mortar. The
216 powder samples (mixed with ZnO) were placed in the holders between two Kapton films. The
217 cylindrical sample diameter and thickness were ~ 10.0 mm and ~ 0.3 mm, respectively. The overall
218 measurement time was ~ 3 h per pattern to have very good statistic over the 2θ range of $5-70^\circ$ with
219 0.0131° step size (2θ).

220 **2.2.4 XRPD data analysis.**

221 Powder patterns of the samples were analyzed by the Rietveld method as implemented in the GSAS
222 software package [38] by using a *pseudo-Voigt* peak shape function [39] with the asymmetry
223 correction included [40] to obtain Rietveld Quantitative Phase Analysis (RQPA). The refined
224 overall parameters were: phase scale factors, background coefficients, unit cell parameters, zero-
225 shift error, peak shape parameters and preferred orientation coefficient, if needed. March-Dollase
226 ellipsoidal preferred orientation correction algorithm was employed [41]. In addition to these
227 parameters, and only for the Rietveld refinements of transmission powder data, a flat-sample
228 absorption coefficient was also optimized as implemented in GSAS. Table 3 reports the crystal
229 structures used in this study to simulate the crystalline phase powder patterns [references 42-59].
230 [The powder diffraction file \(PDF\) codes for all identified phases in the studied cements are also](#)
231 [given in Table 3.](#)

232 The output of a RQPA study for a sample with m-crystalline phases is a set of m-crystalline phase
233 scale factors, $\sum_m S_\alpha$. A phase scale factor, S_α , is related to the phase weight content, W_α , by
234 equation 1 [28].

$$235 \quad S_\alpha = K_e \frac{W_\alpha}{(ZMV)_\alpha \mu_s} \quad (1)$$

236 Where K_e is a constant which depends on the diffractometer operation conditions, μ_s is the sample
237 mass absorption coefficient, Z is the number of chemical units/formulas within the unit cell of α -
238 phase, M is the molecular mass of the chemical formula for α -phase, and V the unit cell volume for
239 α -phase. Once the crystal structure is known, the 'ZMV' term is known. The parameter of interest,
240 W_α , depends on the phase scale factor, S_α , but also on K_e and μ_s . Unfortunately, these two variables
241 are not known and they can not derived from the single powder diffraction pattern of the sample
242 under study.

243 Currently, there are three main ways to derive the phase content, W_α , from the Rietveld refined
244 scale factor, S_α . These three methods are based on different mathematical approaches and they have
245 different experimental complexities. They are very briefly discussed below.

246 **2.2.4.1 Normalization to full crystalline content method.**

247 The simplest approach is the approximation that the sample is only composed of crystalline phases
248 with known structures. These crystal structures are used to compute the powder pattern with any
249 Rietveld program code, in this case GSAS. Under this approximation, W_α is given by equation (2)
250 [28]:

$$251 \quad W_\alpha = \frac{S_\alpha (ZMV)_\alpha}{\sum_{i=1}^m S_i (ZMV)_i} \quad (2)$$

252 The use of equation (2) in RQPA eliminates the need to measure the instrument calibration
253 constant, K_e , and the sample mass absorption coefficient, μ_s . However, the method normalizes the
254 sum of the analysed weight fractions to 1.0. Thus, if the sample contains amorphous phases, and/or
255 some amounts of unaccounted crystalline phases, the analysed weight fractions will be
256 overestimated. This approach is by far the most widely used method in RQPA. However, it must be
257 highlighted that the resulting weight fractions are only accurate if the ACn amount is very small
258 (negligible).

259 2.2.4.2 External standard method (G-factor approach).

260 One possibility to quantify the amount of the ACn content is to use the G-factor approach by
261 employing a suitable **external standard**. In this approach, the diffractometer constant, K_e , is
262 calculated according to equation 3 (in this case the standard was NIST Al_2O_3) [34]:

$$263 \quad G = K_e = S_{st} \frac{\rho_{st} V_{st}^2 \mu_{st}}{W_{st}} \quad (3)$$

264 where S_{st} is the Rietveld scale factor of the (external) standard, ρ_{st} is density of the standard, V_{st} is
265 the unit cell volume of the standard, W_{st} is weight fraction the standard (in our case 100 wt%), all
266 values derived from the Rietveld refinement of the external standard pattern collected in identical
267 conditions than those of the cements. μ_{st} is the mass attenuation coefficient of the standard. This G-
268 factor (the average of three independent measurements) was used to determine the mass
269 concentration of each phase in the RQPA of the Yeelimite-containing cements by equation 4:

$$270 \quad W_{\alpha} = S_{\alpha} \frac{\rho_{\alpha} V_{\alpha}^2 \mu_s}{G} \quad (4)$$

271 This method allowed determining the absolute weight fractions by previously obtaining the
272 diffractometer constant. However, the mass attenuation coefficient of the samples are needed, μ_s .

273 These values were independently determined by X-ray fluorescence analysis from data in Table 2.
274 The calculated G factor for NIST Al₂O₃, as well as selected structural details of the used standard, is
275 given in Table 4. The mass attenuation coefficients (MAC) of the individual oxides (calculated with
276 the HighScore Plus 2.2 program) were given in Table 2. Furthermore, the MAC values of the six
277 studied samples were also given in that Table.

278 **2.2.4.3 Internal standard method.**

279 An alternative method to quantify the ACn content is to use the **internal standard method**. In this
280 approach, the sample is spiked with an appropriate standard that should fulfil at least three
281 conditions. It must have an absorption coefficient close to the sample, negligible ACn content, and
282 small average particle size in order to be easily homogenised with the sample under study. In our
283 case, ZnO was used as internal standard. This compound was selected because its MAC value,
284 50.34 cm²/g, yields a linear attenuation coefficient, 285 cm⁻¹, very similar to those of the analysed
285 cements. Furthermore, its particle size is small, approximately 0.5 μm as determined by scanning
286 electron microscopy; its face-centred crystal structure gives a very simple pattern avoiding strong
287 overlapping with the diffraction lines of the studied cements; and a previous study [60] showed very
288 small, if any, ACn content.

289 A simple Rietveld refinement using the methodology explained in section 2.2.4.1 will yield a set of
290 weight fractions normalized to 100%. However in this case, in addition to the weight fractions of
291 the phases in the sample, the Rietveld refined weight fraction of the standard, R_{st}, is also obtained. It
292 should be kept in mind that the weight fraction added of the internal standard is precisely known,
293 W_{st}. If the sample contains ACn, R_{st} will be (much) larger than W_{st}. From this overestimation, the
294 overall ACn content is derived according to equation (5) [32]:

$$295 \quad \text{ACn} = \frac{1 - W_{\text{st}} / R_{\text{st}}}{100 - W_{\text{st}}} \times 10^4 \% \quad (5)$$

296 Once the overall ACn content of the sample under study, ACn, is known, the initial RQPA can be
297 recalculated to yield the real sample phase contents. All details for these calculations have been
298 already reported [32]. Furthermore, the errors associated to this approach and the optimum amount
299 of standard has been recently discussed [61].

300 **3. Results and discussion.**

301 **3.1. Standard RQPA of Yeelimite-containing clinkers/cement.**

302 Three commercial CSA clinkers (ALIPRE®, BELITH_CS10 and S.A.cement), one CSA cement
303 (CSA_trial) and two laboratory-prepared BCSA clinkers (BCSAF_B0 and BCSAF_B2) have been
304 analyzed by LXRPD. Table 5 reports the direct RQPA results (wt%) obtained for these samples
305 where Rietveld results were normalized to 100% of crystalline phases. These values were obtained
306 from the approach described in section 2.2.4.1, and hence, the presence of an ACn fraction is
307 neglected. Standard deviations are derived from three independent measurements (not the
308 mathematical errors from the Rietveld fits). These three analyses were carried out to different
309 portions of the samples for better averaging (i.e. not recording three patterns for the same sample).
310 Figures 1 to 6 show a selected range of the Rietveld plots for the six studied Yeelimite-containing
311 cements. The major peaks for each phase are labelled.

312 Several conclusions can be drawn from the phase analyses reported in Table 5.

313 I) Yeelimite, ideal stoichiometry $\text{Ca}_4\text{Al}_6\text{O}_{12}(\text{SO}_4)$, is known to crystallise in the tectosilicate sodalite
314 type structure, $\text{Na}_4\text{Al}_3\text{Si}_3\text{O}_{12}\text{Cl}$. Replacement of chloride by sulfate and partial replacement of
315 sodium by calcium gives hauynite, $\text{Na}_3\text{CaAl}_3\text{Si}_3\text{O}_{12}(\text{SO}_4)$. Both sodalite and hauynite minerals are
316 cubic. However, some aluminates with sodalite structure are known to be orthorhombic, for
317 instance $\text{Ca}_4\text{Al}_6\text{O}_{12}(\text{WO}_4)$ [62,63]. Therefore, both orthorhombic and cubic structural descriptions
318 have been included in the control file for the RQPA, see Table 3. It is noteworthy that five out of six
319 studied samples contained a mixture of orthorhombic and cubic sodalite type-structures. Only,

320 BC SAF_B2 sample showed just cubic Yeelimite. We speculate that this is due to the simultaneous
321 presence of Na, Fe and Si within cubic Yeelimite in BC SAF_B2. A deep synthetic and structural
322 study of cubic and orthorhombic $C_4A_3\bar{S}$ -type phases is in progress, including neutron powder
323 diffraction, and it will be reported elsewhere.

324 II) It is also important to identify the belite polymorph and its quantification. Borax addition fully
325 transform β -belite in BC SAF_B0 to fully α'_H -belite in BC SAF_B2, in complete agreement with a
326 previous report [60]. The mechanism for the borax-activation of belite has been very recently
327 unravel as a solid solution, $Ca_{2-x}Na_x(SiO_4)_{1-x}(BO_3)_x$, has been proved and the crystal structure of
328 α'_H - $Ca_{1.85}Na_{0.15}(SiO_4)_{0.85}(BO_3)_{0.15}$ has been worked out [45]. It is also noteworthy that S.A.cement
329 has a high α'_H -belite content. This can be justified with the elemental composition reported in Table
330 2, as its Na_2O content is quite high, 1.4 wt%. Na_2O is known to stabilise α -forms of belite [64,65].

331 III) CS quantified in ALIPRE®, S.A.cement and CSA_trial is the high temperature polymorph,
332 anhydrite-II [48]. So, this less reactive CS was likely produced during the clinkering process. It
333 should be noted that gypsum, bassanite and less-soluble anhydrite-II can be easily distinguished and
334 quantified by RQPA. However, bassanite and highly soluble anhydrite-III can only be distinguished
335 in especial experimental conditions [66] with high-quality laboratory X-ray powder diffraction data.

336 IV) The good accuracy of the analyses can be estimated by the comparison of the XRF results
337 (Table 2) and RQPA results (Table 5). RQPA showed the highest amount of periclase (MgO) for
338 BELITH_CS10, 2.2(2) wt%, and this is in full agreement with elemental analysis reported in Table
339 2, where this clinker showed the highest MgO content, 2.7 wt%. Furthermore, S.A.cement was the
340 second sample with the highest magnesium content determined by XRF, 1.5 wt%, and RQPA
341 showed the second highest periclase content, 1.1 wt%. We choose to compare magnesium oxide
342 contents because magnesium is little soluble in the Yeelimite structure.

343 V) The presence of ternesite (also known as sulfate-spurrite), C_5S_2S , is quite uncommon in CSA or
344 BCSA clinkers. However, CSA_trial has a high amount of ternesite, 16.2(5) wt%. This is likely due
345 to a very high SO_3 dosage in the raw materials. XRF SO_3 value for this cement, 16.7 wt%, is very
346 high even taken into account the ~14 wt% of gypsum added. Overall SO_3 values range
347 approximately from 9 to 14 wt% for CSA clinkers and between 3 and 4 wt% for BCSA clinkers.

348 VI) Titanium is usually present in CSA and BCSA cements as it accompanies aluminium in
349 bauxites. High aluminium contents in CSA clinkers are linked to high titanium contents as shown in
350 Table 2. Consequently, lower aluminium contents in BCSA are linked to lower titanium contents.
351 Furthermore, titanium may replace aluminium in some phases but the solubility limits are exceeded
352 in CSA and BCSA clinkers. This is evident from the RQPA as the perovskite $CaTiO_3$ phase
353 segregates. We have carried out the RQPA with this assumed stoichiometry, $CaTiO_3$, however
354 further studies are needed in order to establish the stoichiometry of the perovksite phase as it is very
355 well known that this phase forms extensive solid solutions with transition metals.

356 Finally, selective dissolutions have been carried out for BCSAF_B0 and BCSAF_B2, see Figures 7
357 and 8. This work was carried out for a better characterisation of these samples. For instance, it can
358 be highlighted that the main peak of CT is strongly overlapped with the main peak of C_3A and
359 merwinite, $Ca_3Mg(SiO_4)_2$. Therefore, RQPA, itself, can not distinguish between these phases.
360 Figure 7 shows a small selected region of the Rietveld plots for BCSAF_B0 clinker plus the
361 aluminate and silicate residues. Figure 8 shows the same type of graphic for BCSAF_B2. The
362 Rietveld plot for the silicate residue of BCSAF_B0 is very informative as the diffraction peaks from
363 C_4AF disappear but the diffraction peak at $\sim 33.3^\circ$ (2θ) is still present. Hence, this phase could be
364 perovskite or merwinite but not C_3A . The Rietveld refinements of the silicate residue indicated that
365 the fit with perovskite was better (lower R-factors) than that with merwinite.

366 Furthermore, a close analysis of the Rietveld plots of the residues indicates that the peaks widths in
367 the BC SAF_B2 are narrower than those in BC SAF_B0. For instance, the diffraction peaks from CT
368 and C_4A_3S in BC SAF_B2 aluminate fraction are narrower than those in the BC SAF_B0 aluminate
369 fraction, see Figure 8b and 7b, respectively. This behaviour is likely due to a better particle growth
370 when borax is added. In fact, scanning electron microscopy data (not shown) indicate that the
371 average particle sizes for BC SAF_B2 are larger than those of BC SAF_B0. However, the unit cell
372 values of some phases change between the two studied clinkers. Furthermore, these values also
373 slightly change between a clinker and the residues. So, the unit cell variations may also influence
374 the degree of overlapping and consequently, some peak widths.

375 **3.2. Absolute RQPA of Yeelite-containing clinkers/cement.**

376 Table 6 shows the RQPA results (wt%) for the Yeelite-containing samples including the ACn
377 contents employing the two methodologies previously described. The values obtained from
378 reflection geometry using an external standard (G-method) are given in the first row. The values
379 obtained from transmission geometry using ZnO as internal standard are given in the second row. In
380 both cases, standard deviations are derived from three independent measurements.

381 Three important conclusions can be drawn from the comparative study shown in Table 6. Firstly,
382 using the G-factor (previously obtained with an external standard, see Table 4), it allowed
383 measuring both the crystalline phases and the ACn contents. The ACn contents of CSA
384 clinkers/cements are similar to those found in OPC cements, ~ 10 wt% [30-32]. However, these
385 contents are much higher in BC SA clinkers, of the order of 25 wt%. We would like to highlight that
386 this measurement does not mean that there is about 25 wt% of amorphous/sub-cooled liquid in these
387 clinkers. These high values are likely due to the high concentration of impurities and defects in
388 belite.

389 Secondly, transmission powder diffraction data were also recorded for the same samples. An
390 alternative methodology is always advisable to show the appropriateness of data recording and data
391 analysis strategies. Furthermore, although the internal standard dilutes the phases in the samples,
392 ZnO was added to determine the overall ACn contents. Table 6 also reports the analytical results
393 obtained from this methodology. Overall, the same trend was obtained concerning the ACn
394 contents. CSA clinkers have ACn contents close to 10 wt% except for BELITH_CS10, which
395 essentially had a zero value. Furthermore, the BCSA clinkers displayed high ACn contents, ~ 25
396 wt%, in full agreement with those obtained with the G-method.

397 For the internal standard method, the reported uncertainties in Table 6 are those arising from the
398 average of three measurements. However, the uncertainties resulting from the amount of standard
399 used, 25 wt%, are not taken into account. Therefore, the standard deviations reported for the ACn
400 numbers are underestimated. Errors close to 3 wt% are more likely to occur, but they are very
401 difficult to quantify with precision.

402 Thirdly, a brief discussion on the results obtained by these two methods is worthy, see Table 6. For
403 four samples, S.A.cement, CSA_trial, BCSA_B0 and BCSAF_B2, the Rietveld quantitative phase
404 analysis values agree quite well. However, for ALIPRE® and BELITH_CS10, the results are not
405 that satisfactory. For ALIPRE®, the differences in the quantification of C_4A_3S-c , β -belite and ACn
406 are 5.7, 4.3 and 10.3 wt%. Three times the standard deviations is commonly used for a good level of
407 confidence. So, the sum of 3σ for the two analyses was calculated giving 3.0, 5.1 and 9.6 wt% for
408 C_4A_3S-c , β -belite and ACn values, respectively. Therefore, the quantification of C_4A_3S-c for
409 ALIPRE® is well out of the limits. For BELITH_CS10, the differences in the quantification of
410 C_4A_3S-o , β -belite and ACn are 4.3, 7.2 and 14.5 wt%, with the sum of 3σ for the two analyses
411 giving 3.9, 3.9 and 5.7 wt%, respectively. In this case, the quantification of β -belite and ACn does

412 not agree. We do not have a definitive answer for this behaviour but correlations of the phase scale
413 factors with the peak shape parameters may be likely playing a role.

414 Finally, it is worth to highlight the importance of having accurate structural description for every
415 phase in the cements to be analysed. This is more important for high-content phases, and it will be
416 illustrated for the RQPA of BC SAF_B2. If the 'old' approximate crystal structure of $\alpha'_H\text{-C}_2\text{S}$ is
417 used [44], one Rietveld fit of the reflection data gave $R_{\text{WP}}=5.22\%$ and $R_{\text{F}}(\alpha'_H\text{-C}_2\text{S})=7.24\%$. The
418 application of the G-method gave $\alpha'_H\text{-C}_2\text{S}$ and ACn contents of 35 and 33 wt%, respectively. If a
419 better structural description is used, $\alpha'_H\text{-Ca}_{1.85}\text{Na}_{0.15}(\text{SiO}_4)_{0.85}(\text{BO}_3)_{0.15}$ [45], then, the Rietveld fit of
420 the same pattern was better (lower disagreement factors): $R_{\text{WP}}=4.87\%$ and $R_{\text{F}}(\alpha'_H\text{-C}_2\text{S})=5.72\%$.
421 This better fit gave a larger $\alpha'_H\text{-C}_2\text{S}$ scale factor (30.94 instead of 25.53) and therefore, the $\alpha'_H\text{-C}_2\text{S}$
422 content was larger (40 wt%) and ACn content smaller, 28 wt%. So, the use of approximate crystal
423 structures give lower determined crystalline phase contents and higher ACn contents, as expected.

424

425 **4. Conclusions.**

426 Rietveld quantitative phase analyses of three commercially-available calcium sulfoaluminate
427 clinkers have been successfully carried out. In addition, two laboratory prepared iron-rich belite
428 calcium sulfoaluminate clinkers have been also studied. All commercial CSA clinkers contained
429 mixtures of orthorhombic and cubic Yeelimites. Only, the borax-activated BC SA clinker contained
430 just cubic-Yeelimate. Moreover borax addition transform β -belite in BC SAF_B0 to fully α'_H -belite
431 in BC SAF_B2. Other accompanying phases have been quantified. It has been found a good
432 agreement between elemental compositions obtained by X-ray fluorescence and mineralogical
433 compositions obtained by Rietveld analysis of powder diffraction data as shown for MgO/periclase.
434 Selective dissolutions were employed to better characterise the iron-rich belite calcium

435 sulfoaluminate clinkers. Using this approach, every phase in the samples was firmly established.
436 Finally, the ACn contents of these materials were measured by both external and internal standard
437 methods. The agreement was fairly good for some cements but the variations for ALIPRE® and
438 BELITH_CS10 were larger than expected. Overall, the analyses showed that the commercial
439 calcium sulfoaluminate clinkers have ACn contents quite similar to those of OPCs, ~ 10 wt%.
440 Conversely, the ACn contents of the belite calcium sulfoaluminate clinkers were higher, ~ 25 wt%.

441 **Acknowledgments**

442 This work has been supported by Spanish Ministry of Science and Innovation through MAT2010-
443 16213 research grant, which is co-funded by FEDER. I.S. thanks a Ramón y Cajal fellowship,
444 RYC-2008-03523.

445 **References**

- 446 [1] A. Klein, Calciumaluminosulfate and expansive cements containing same, US Patent No. 3,
447 155, 526 (1963) 4 pp.
- 448 [2] Y. Wang, M. Su, The third cement series in China, World Cem. 25 (1994) 6-10.
- 449 [3] E.M. Gartner, Industrially interesting approaches to “low- CO₂” cements, Cem. Concr. Res. 34
450 (2004) 1489-1498.
- 451 [4] G.S. Li, G. Walenta, E.M. Gartner, Formation and hydration of low-CO₂ cements based on
452 belite, calcium sulfoaluminate and calcium aluminoferrite, Proceedings of the 12th ICCI, Montreal,
453 Canada (2007) pp TH3-15.3.
- 454 [5] M.C.G. Juenger, F. Winnefeld, J.L. Provis, J.H. Ideker, Advances in alternative cementitious
455 binders, Cem. Concr. Res. 41 (2011) 1232-1243.
- 456 [6] Q. Zhou, N.B. Milestone, M. Hayes, An alternative to Portland cement for waste
457 encapsulation—the calcium sulfoaluminate cement system, J. Hazard. Mater. 136 (2006) 120–129.

- 458 [7] F.P. Glasser, L. Zhang, High-Performance Cement Matrices Based on Calcium
459 Sulphoaluminate-Belite Compositions, *Cem. Concr. Res.* 31 (2001) 1881-1886.
- 460 [8] J. Beretka, M. Marroccoli, N. Sherman, G.L. Valenti, The influence of C_4A_3S content and WS
461 ratio on the performance of calcium sulfoaluminate-based cements, *Cem. Concr. Res.* 26 (1996)
462 1673-1681.
- 463 [9] S. Sahu, J. Majling, Preparation of sulphoaluminate belite cement from fly ash, *Cem. Concr.*
464 *Res.* 24 (1994) 1065-1072.
- 465 [10] I. Odler, *Special inorganic cements*, Taylor and Francis Publisher. Cap. 4 (2000) 69-74.
- 466 [11] F. Winnefeld, S. Barlag, Calorimetric and thermogravimetric study on the influence of calcium
467 sulfate on the hydration of yeelimite, *J. Therm. Anal. Calorim.* 101 (2010) 949-957.
- 468 [12] S. Berger, C.C.D. Coumes, P. Le Bescop, D. Damidot, Influence of a thermal cycle at early age
469 on the hydration of calcium sulphoaluminate cements with variable gypsum contents, *Cem. Concr.*
470 *Res.* 41 (2011) 149-160.
- 471 [13] I.A. Chen, C.W. Hargis, M.C.G. Juenger, Understanding expansion in calcium sulfoaluminate-
472 belite cements, *Cem. Concr. Res.* 42 (2012) 51-60.
- 473 [14] L. Zhang, F.P. Glasser, Hydration of calcium sulfoaluminate cement at less than 24 h, *Adv.*
474 *Cem. Res.* 14 (2002) 141-155.
- 475 [15] G.S. Li, E.M. Gartner, High-belite sulfoaluminate clinker: fabrication process and binder
476 preparation, World Patent Application WO 2006/018569 A2.
- 477 [16] K. Quillin, Performance of belite-sulfoaluminate cements, *Cem. Concr. Res.* 31 (2001) 1341-
478 1349.
- 479 [17] I. Janotka, U. Krajci, S.C. Mojumdar, Performance of sulphoaluminate-belite cement with high
480 C_4A_3S content, *Ceram. Silik.* 51 (2007) 74-81.
- 481 [18] D. Adolfsson, N. Menad, E. Viggh, B. Bjorkman, Hydraulic properties of sulphoaluminate
482 belite cement based on steelmaking slags, *Adv. Cem. Res.* 19 (2007) 133-138.

- 483 [19] J. Pera, J. Ambroise, New applications of calcium sulfoaluminate cement, *Cem. Concr. Res.* 34
484 (2004) 671-676.
- 485 [20] G. Walenta, C. Comparet, V. Morin, E. Gartner, Hydraulic binder based on sulfoaluminate
486 clinker and minerals additions, World Patent Application WO 2010/070215 A1 (2010).
- 487 [21] G. Walenta, E. Gartner, V. Morin, Additives for hydraulic binder based on iron-rich belite
488 calcium sulfoaluminate clinker, World Patent Application WO 2011/020958 A1 (2011).
- 489 [22] A. Wolter, Belite cements and low energy clinker, *Cem. Inter.* 3 (2005) 106-117.
- 490 [23] G.L. Valenti, M. Marroccoli, F. Montagnaro, M. Nobili, A. Telesca, Synthesis, hydration
491 properties and environmental friendly features of calcium sulfoaluminate cements, Proceedings of
492 the 12th International Congress of Cement Chemistry, Montreal (2007) W3 11.2.
- 493 [24] M.C Martín-Sedeño, A.J.M. Cuberos, A.G. De la Torre, G. Álvarez-Pinazo, L.M. Ordóñez, M.
494 Gateshki, M.A.G. Aranda, Aluminum-rich belite sulfoaluminate cements: Clinkering and early age
495 hydration, *Cem. Concr. Res.* 40 (2010) 359–369.
- 496 [25] A.G. De la Torre, A.J.M. Cuberos, G. Alvarez-Pinazo, A. Cuesta, M.A.G. Aranda, In situ
497 powder diffraction study of belite sulfoaluminate clinkering, *J. Synchr. Rad.* 18 (2011) 506–514.
- 498 [26] J. Li, H. Ma, H. Zhao, Preparation of Sulphoaluminate-alite Composite Mineralogical Phase
499 Cement Clinker from High Alumina Fly Ash, *Key Eng. Mat.* 334-335 (2007) 421–424.
- 500 [27] H.M. Rietveld, A Profile Refinement Method for Nuclear and Magnetic Structures, *J. Appl.*
501 *Cryst.* 2 (1969) 65-71.
- 502 [28] D.L. Bish, S.A. Howard SA, Quantitative phase analysis using the Rietveld method, *J. Appl.*
503 *Cryst.* 21 (1988) 86-91.
- 504 [29] O. Pritula, L. Smrcok, B. Baumgartner, On reproducibility of Rietveld analysis of reference
505 Portland cement clinkers, *Pow. Diffr.* 18 (2003) 16-22.
- 506 [30] P.M. Suherman, A.V. Riessen, B. O’connor, D. Li, D. Bolton, H. Fairhurst, Determination of
507 amorphous phase levels in Portland cement clinker, *Pow. Diffr.* 17 (2002) 178-185.

508 [31] P.S. Whitfield, L.D. Mitchell, Quantitative Rietveld analysis of the amorphous content in
509 cements and clinkers, *J. Mater. Sci.* 38 (2003) 4415-4421.

510 [32] A.G. De la Torre, S. Bruque, M.A.G. Aranda, Rietveld quantitative amorphous content
511 analysis, *J. Appl. Cryst.* 34 (2001) 196-202.

512 [33] J.P. Cline, R.B. Von Dree, R. Winburn, P.W. Stephens, J.J. Filliben, Addressing the
513 amorphous content issue in quantitative phase analysis: the certification of NIST standard reference
514 material 676a, *Acta Cryst. Sect A* 67 (2011) 357-367.

515 [34] B.H. O'Connor, M.D. Raven, Application of the Rietveld refinement procedure in assaying
516 powdered mixtures, *Pow. Diffr.* 3 (1988) 2-6.

517 [35] D. Jansen, Ch. Stabler, F. Goetz-Neunhoeffler, S. Dittrich, J. Neubauer, Does Ordinary Portland
518 Cement contain amorphous phase? A quantitative study using an external standard method, *Pow.*
519 *Diffr.* 26 (2011) 31-38.

520 [36] D. Jansen, F. Goetz-Neunhoeffler, B. Lothenbach, J. Neubauer, The early hydration of Ordinary
521 Portland Cement (OPC): An approach comparing measured heat flow with calculated heat flow
522 from QXRD, *Cem. Concr. Res.* 42 (2012) 134-138.

523 [37] J. Wang, Hydration mechanism of cements based on low-CO₂ clinkers containing belite,
524 ye'elimite and calcium alumino-ferrite, PhD Thesis, University of Lille (2010).

525 [38] A.C. Larson, R.B. Von Dreele, General Structure Analysis System (GSAS), Los Alamos
526 National Laboratory Report LAUR (2000) pp 86-748.

527 [39] P. Thompson, D.E. Cox, J.B. Hasting, Rietveld refinement of Debye-Scherrer synchrotron X-
528 ray data from Al₂O₃, *J. Appl. Cryst.* 20 (1987) 79-83.

529 [40] L.W. Finger, D.E. Cox, A.P. Jephcoat, A correction for powder diffraction peak asymmetry
530 due to diaxial divergence, *J. Appl. Cryst.* 27 (1994) 892-900.

531 [41] W.A. Dollase, Correction of intensities for preferred orientation in powder diffractometry:
532 application of the March model, *J. Appl. Cryst.* 19 (1986) 267-272.

533 [42] N.J. Calos, C.H.L. Kennard, A.K. Whittaker, R.L.Davis, Structure of calcium aluminate
534 sulphate $\text{Ca}_4\text{Al}_6\text{O}_{16}\text{S}$, *J. Solid State Chem.* 119 (1995) 1-7.

535 [43] H. Saalfeld, W.Depmeier, Silicon-free compounds with sodalite structure, *Kristall und*
536 *Technik*, 7 (1972) 229-233.

537 [44] W.G. Mumme, R.J. Hill, G. Bushnell-Wye, E.R. Segnit, Rietveld crystal structure refinement,
538 chemistry and calculated powder diffraction data for the polymorphs of dicalcium silicate and
539 related phases, *N. Jb. Miner. Abh.* 169 (1995) 35-68.

540 [45] A. Cuesta, E.R. Losilla; M.A.G. Aranda, A.G. De la Torre, Reactive belite stabilization
541 mechanisms by boron-bearing dopants, *Cem. Concr. Res.* 42 (2012) 598-606.

542 [46] A.A. Colville, S. G  ller, The crystal structure of brownmillerite, $\text{Ca}_2\text{FeAlO}_5$, *Acta Cryst. B27*
543 (1971) 2311-2315.

544 [47] S. Sasaki, C.T. Prewitt, J.D.Bass, Orthorhombic perovskite CaTiO_3 and CdTiO_3 : structure and
545 space group, *Acta Cryst. C43* (1987) 1668-1674.

546 [48] A. Kirfel, G. Will, Charge density in anhydrite, CaSO_4 , from X-ray and neutron diffraction,
547 *Acta Cryst. B36* (1980) 2881-2890.

548 [49] A.G. De la Torre, M.G. Lopez-Olmo, C. Alvarez-Rua, S. Garcia-Granda, M.A.G. Aranda,
549 Structure and microstructure of gypsum and its relevance to Rietveld quantitative phase analyses,
550 *Pow. Diffr.* 19 (2004) 240-246.

551 [50] S. Sasaki, K. Fujino, Y. Takeuchi, X-ray determination of electron-density distributions in
552 oxides, MgO , MnO , CoO , and NiO , and atomic scattering factors of their constituent atoms, *Proc.*
553 *Jap. Acad.* 55 (1979) 43-48.

554 [51] W. H  rkner, Hk. M  ller-Buschbaum, Crystal-structure of CaAl_2O_4 , *Inorg. Nuclear Chem.* 38
555 (1976) 983-984.

556 [52] A.G. De la Torre, S. Bruque, J. Campo, M.A.G. Aranda, The superstructure of C_3S from
557 synchrotron and neutron powder diffraction and its role in quantitative phase analyses, *Cem. Concr.*
558 *Res.* 32 (2002) 1347-1356.

559 [53] S.J. Louisnathan, Refinement of the crystal structure of a natural gehlenite, $Ca_2Al(Al,Si)O_7$,
560 *Can. Min.* 10 (1971) 822-837.

561 [54] P.D. Brotherton, J.M. Epstein, M.W. Pryce, A.H. White, Crystal structure of calcium
562 sulphosilicate, $Ca_5(SiO_4)_2(SO_4)$, *Australian J. Chem.* 27 (1974) 657-660.

563 [55] H. Effenberger, A. Kirfel, G. Wil, Studies of the electron-density distribution of dolomite,
564 $CaMg(CO_3)_2$, *Tschermaks Mineralogische und Petrographische Mitteilungen*, 31 (1983) 151-164.

565 [56] I.P. Swainson, , M.T. Dove, W.W.Schmahl, A. Putnis, Neutron Diffraction Study of the
566 Akermanite-Gehlenite Solid Solution Series, *Phys. Chem. Min.* 19 (1992) 185-195.

567 [57] V. Kahlenberg, G. Doersam, M. Wendschuh-Josties, R.X. Fischer, The crystal structure of
568 delta- $(Na_2Si_2O_5)$, *J. Solid State Chem.* 146 (1999) 380-386.

569 [58] E.N. Maslen, V.A. Streltsov, N.R. Streltsova, N. Ishizawa, Y. Satow, Synchrotron X-ray study
570 of the electron density in alpha- Al_2O_3 , *Acta Cryst.* B49 (1993) 973-980.

571 [59] J. Albertsson, S.C. Abrahams, A. Kvik, Atomic displacement, anharmonic thermal vibration,
572 expansivity and pyroelectric coefficient thermal dependences in ZnO, *Acta Cryst.* B45 (1989) 34-
573 40.

574 [60] A.J.M. Cuberos, A.G. De la Torre, G. Álvarez-Pinazo, M.C. Martín-Sedeño, K. Schollbach, H.
575 Pöllmann, M.A.G. Aranda, Active Iron-Rich Belite Sulfoaluminate Cements: Clinkering and
576 Hydration, *Environ. Sci. Technol.* 44 (2010) 6855-6862.

577 [61] T. Westphal, T. Füllmann, H. Pöllmann, Rietveld quantification of amorphous portions with an
578 internal standard-mathematical consequences of the experimental approach, *Pow. Diffr.* 24 (2009)
579 239-243.

580 [62] W. Depmeier, Aluminate Sodalite $\text{Ca}_8[\text{Al}_{12}\text{O}_{24}](\text{WO}_4)_2$ at Room Temperature, *Acta Cryst.* C40
581 (1984) 226-231.

582 [63] W. Depmeier, Structure of Cubic Aluminate Sodalite $\text{Ca}_8[\text{Al}_{12}\text{O}_{24}](\text{WO}_4)_2$ in Comparison with
583 its Orthorhombic Phase and with Cubic $\text{Sr}_8[\text{Al}_{12}\text{O}_{24}](\text{CrO}_4)_2$, *Acta Cryst.* B44 (1988) 201-207.

584 [64] K. Morsli, AG. de la Torre, S. Stober, A.J.M. Cuberos, M. Zahir, M.A.G. Aranda, Quantitative
585 Phase Analysis of Laboratory-Active Belite Clinkers by Synchrotron Powder Diffraction, *J. Am.*
586 *Ceram. Soc.* 90 (2007) 3205-3212.

587 [65] K. Morsli, AG. de la Torre, M. Zahir, M.A.G. Aranda, Mineralogical phase analysis of alkali
588 and sulfate bearing belite rich laboratory clinkers, *Cem. Concr. Res.* 37 (2007) 639-646.

589 [66] S. Seufert, C. Hesse, F. Goetz-Neunhoeffer, J. Neubauer, Discrimination of bassanite and
590 anhydrite III dehydrated from gypsum at different temperatures, *Z. Kristallogr. Suppl.* 30 (2009)
591 447-452.

592

593

594 **Figure Captions**

595 **Figure 1.** Selected range of the Rietveld plot for ALIPRE® clinker. Crosses are the experimental
596 scan, solid line is the calculated pattern and the bottom line is the difference curve. The major peaks
597 for each phase are labelled.

598 **Figure 2.** Selected range of the Rietveld plot for BELITH_CS10 clinker. Crosses are the
599 experimental scan, solid line is the calculated pattern and the bottom line is the difference curve.
600 The major peaks for each phase are labelled.

601 **Figure 3.** Selected range of the Rietveld plot for S.A.cement clinker. Crosses are the experimental
602 scan, solid line is the calculated pattern and the bottom line is the difference curve. The major peaks
603 for each phase are labelled.

604 **Figure 4.** Selected range of the Rietveld plot for CSA_trial cement. Crosses are the experimental
605 scan, solid line is the calculated pattern and the bottom line is the difference curve. The major peaks
606 for each phase are labelled.

607 **Figure 5.** Selected range of the Rietveld plot for BC SAF_B0 clinker. Crosses are the experimental
608 scan, solid line is the calculated pattern and the bottom line is the difference curve. The major peaks
609 for each phase are labelled.

610 **Figure 6.** Selected range of the Rietveld plot for BC SAF_B2 clinker. Crosses are the experimental
611 scan, solid line is the calculated pattern and the bottom line is the difference curve. The major peaks
612 for each phase are labelled.

613 **Figure 7.** Selected small range ($30 - 36^\circ / 2\theta$) of the Rietveld plots for: (a) BC SAF_B0 clinker, (b)
614 BC SAF_B0 aluminate residue, (c) BC SAF_B0 silicate residue. All details as in previous Rietveld
615 figures.

616 **Figure 8.** Selected small range ($30 - 36^\circ / 2\theta$) of the Rietveld plots for: (a) BC SAF_B2 clinker, (b)
617 BC SAF_B2 aluminate residue, (c) BC SAF_B2 silicate residue. All details as in previous Rietveld
618 figures.

619

620

Table 1. Raw materials employed for the preparation of BCSAF clinkers (expressed in grams).

	Limestone	Kaolin	Bauxite	Gypsum	Marl	Borax
BCSAF_B0	1796.30	281.03	519.53	227.51	209.78	-
BCSAF_B2	1744.21	272.88	504.47	220.91	203.70	120.26

Table 2. Elemental composition, determined by XRF and expressed as oxide wt%, of the Yeelimite-containing clinkers. The mass attenuation coefficients (MAC) used in this study are also given in italics.

	ALIPRE®	BELITH_CS10	S.A.cement	CSA_trial	BCSAF_B0	BCSAF_B2	<i>MAC (cm²/g)</i>
CaO	41.59	41.86	44.10	45.59	51.75	50.99	<i>120.47</i>
Al₂O₃	33.64	33.85	27.30	20.93	18.78	17.03	<i>30.91</i>
SiO₂	6.52	8.21	9.00	10.13	16.70	16.53	<i>34.84</i>
SO₃	13.97	8.81	12.20	16.66	3.68	3.70	<i>42.48</i>
Fe₂O₃	0.89	2.37	2.60	3.63	6.72	6.28	<i>220.77</i>
B₂O₃[#]	-	-	-	-	0.13	2.37	<i>8.26</i>
Na₂O[#]	0.09	<0.08	1.40	0.18	0.10	1.00	<i>24.28</i>
K₂O	0.39	0.25	0.30	0.31	0.34	0.33	<i>116.82</i>
MgO	0.68	2.73	1.50	1.26	0.99	0.97	<i>27.88</i>
TiO₂	1.48	1.50	1.30	1.00	0.65	0.62	<i>121.97</i>
SrO	0.50	0.15	0.20	0.17	0.028	0.03	<i>100.36</i>
Cr₂O₃	-	0.017	-	0.02	0.028	0.023	<i>176.40</i>
MnO	-	0.011	-	0.02	0.036	0.034	<i>217.87</i>
ZrO₂	0.10	0.070	-	0.05	0.021	0.019	<i>104.15</i>
P₂O₅	0.16	0.13	0.10	0.04	0.055	0.059	<i>38.59</i>
<i>MAC (cm²/g)</i>	<i>73.81</i>	<i>75.96</i>	<i>78.56</i>	<i>82.31</i>	<i>92.00</i>	<i>89.28</i>	-

B₂O₃ and Na₂O contents were measured by ICP-MS.

Table 3. ICDD-PDF and ICSD collection codes for all phases used for Rietveld refinements.

	PDF-code	ICSD code	Ref.		PDF-code	ICSD code	Ref.
C_4A_3S-o	01-085-2210	80361	[42]	M	01-071-1176	9863	[50]
C_4A_3S-c	01-071-0969	9560	[43]	CA	01-070-0134	260	[51]
$\gamma-C_2S$	01-086-0397	81095	[44]	C₃S	01-070-8632	94742	[52]
$\beta-C_2S$	01-086-0398	81096	[44]	C₂AS	01-089-5917	87144	[53]
$\alpha'-C_2S$	01-086-0399	81097	[44]	C₅S₂S	01-070-1847	4332	[54]
$\alpha'-C_2S$ (act.)	01-086-0399	-	[45]	Dolomite	01-075-1711	31277	[55]
C₄AF	01-071-0667	9197	[46]	Akermanite	01-079-2425	67691	[56]
CT	01-078-1013	62149	[47]	Na₂Si₂O₅	01-089-8339	88662	[57]
CS	01-072-0916	16382	[48]	Al₂O₃ (standard)	01-081-2267	73725	[58]
CSH₂	00-033-0311	151692	[49]	ZnO (standard)	01-079-0206	65120	[59]

Table 4. Computed G factor and selected structural details for the alumina standard used.

Rietveld scale factor from GSAS program[#]	236.60 [#]
S_{st} (NIST Al₂O₃)	0.92748
Cell volume	2.551·10 ⁻²² (cm ³)
Density	3.998 (g/cm ³)
MAC	30.91 (cm ² /g)
G-factor	7.46·10 ⁻⁴² (cm ⁵ /wt%)

[#] The individual phase scale factors provided in the GSAS program output are multiplied by each phase volume (in Å³). So, this has to be taken into account when using equations 3 and 4.

Table 5. Direct RQPA results (wt%) for the Yeelimite-containing clinkers normalized to 100% of crystalline phases. Standard deviations are derived from three independent measurements (not the mathematical errors from the Rietveld fit).

	C_4A_3S-o	C_4A_3S-c	$\alpha'-C_2S$	$\beta-C_2S$	C_4AF	CT	M	C_5S_2S	CSH_2	CS	C_3S
ALIPRE®¹	51.0(7)	18.5(6)	9.4(3)	7.7(1)		3.5(1)	0.52(2)			9.0(4)	
BELITH_CS10²	40.1(9)	25.5(6)		16.0(2)	2.4(1)	9.3(1)	2.2(2)				
S.A.cement³	27.5(5)	28.7(6)	21.4(9)	9.7(4)		3.5(4)	1.1(1)			6.3(1)	
CSA_trial⁴	16.5(1.3)	23.6(7)		9.0(9)		4.8(2)		16.2(5)	13.7(4)	8.5(2)	5.9(5)
BCSAF_B0⁵	14.6(1.1)	13.5(1.2)		48.7(6)	14.9(2)	1.3(2)					
BCSAF_B2		31.1(1.7)	56.7(1.8)		10.1(6)	2.1(2)					

²Also contains 4.6(1) wt% of akermanite.

³Also contains 1.9(1) wt% of CA.

⁴Also contains 1.8(7) wt% of dolomite.

⁵Also contains 2.6(5) wt% of $\gamma-C_2S$ and 4.4(2) wt% of C_2AS .

Table 6. RQPA results (wt%) for the Yeelimite-containing clinkers including the overall amorphous plus not-quantified crystalline phase(s) content. The values obtained from reflection geometry using an external standard (G-method) are given in the first row. The values obtained from transmission geometry using ZnO as internal standard are given in the second row (italics). Standard deviations are derived from three independent measurements (not the mathematical errors from the Rietveld fit).

	C_4A_3S-o	C_4A_3S-c	$\alpha'-C_2S$	$\beta-C_2S$	C_4AF	CT	M	C_5S_2S	CSH_2	CS	C_3S	ACn [#]
ALIPRE®¹	42.0(9)	15.3(5)	7.7(2)	6.4(1)		2.9(1)	0.43(1)			7.5(4)		17.5(1.4)
	<i>41.0(8)</i>	<i>21.0(5)</i>	<i>7.6(2)</i>	<i>10.7(1.6)</i>		<i>3.0(2)</i>	<i>0.5(2)</i>			<i>8.2(1)</i>		<i>7.2(1.8)</i>
BELITH_CS10²	35.8(4)	22.8(3)		14.3(3)	2.1(1)	8.3(2)	2.0(2)					10.6(8)
	<i>40.1(9)</i>	<i>23.0(9)</i>		<i>21.5(1.0)</i>	<i>2.1(4)</i>	<i>7.9(1)</i>	<i>2.1(1)</i>					<i>-3.9(1.1)</i>
S.A.cement³	24.2(6)	25.3(9)	18.8(4)	8.6(5)		3.1(4)	0.92(2)			5.6(2)		11.9(1.7)
	<i>23.0(7)</i>	<i>27.2(6)</i>	<i>17.1(3)</i>	<i>8.8(6)</i>		<i>2.9(1)</i>	<i>0.7(1)</i>			<i>6.1(1)</i>		<i>13.5(6)</i>
CSA_trial⁴	14.6(7)	21.2(1.0)		8.0(1.1)		4.3(3)		14.4(8)	12.2(7)	7.6(1)	5.3(6)	10.8(2.9)
	<i>14.3(6)</i>	<i>20.7(8)</i>		<i>9.0(6)</i>		<i>3.4(2)</i>		<i>13.0(1)</i>	<i>13.3(3)</i>	<i>7.5(2)</i>	<i>6.0(6)</i>	<i>12.3(1.4)</i>
BCSAF_B0⁵	10.9(1.0)	10.0(8)		36.2(1.3)	11.1(2)	1.0(1)						25.5(2.1)
	<i>10.2(7)</i>	<i>8.8(6)</i>		<i>33.3(1)</i>	<i>12.9(3)</i>	<i>0.6(2)</i>						<i>26.1(4)</i>
BCSAF_B2		22.5(1.6)	40.9(1.0)		7.3(4)	1.5(2)						27.7(1.2)
		<i>22.1(3)</i>	<i>41.9(4)</i>		<i>10.3(2)</i>	<i>0.9(2)</i>						<i>24.9(9)</i>

[#] ACn stands for amorphous plus not-quantified crystalline phase(s) which includes misfitting problems and not-computed phase(s).

¹ Also contains: 0.4(1) wt% $Na_2Si_2O_5$. *0.8(3) wt% $Na_2Si_2O_5$.*

² Also contains: 4.1(1) wt% akermanite. *7.3(1) wt% akermanite.*

³ Also contains 1.6(1) wt% CA. *0.8(2) wt% CA*

⁴ Also contains 1.6(5) wt% dolomite. *1.0(4) wt% dolomite*

⁵ Also contains 1.9(4) wt% $\gamma-C_2S$ and 3.3(2) wt% C_2AS . *1.5(2) wt% $\gamma-C_2S$ and 6.7(3) wt% C_2AS .*

Figure(s)

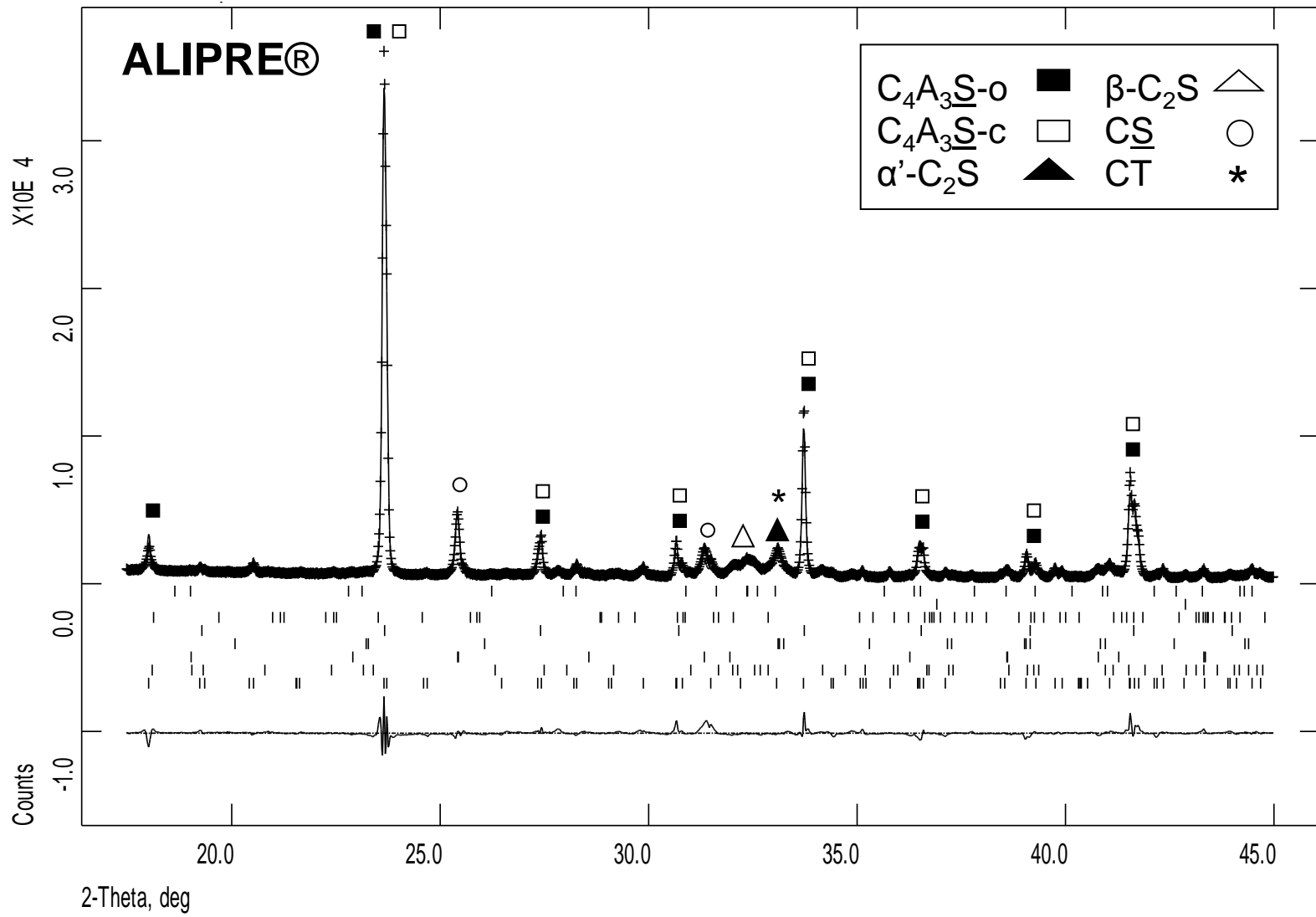


Figure 1

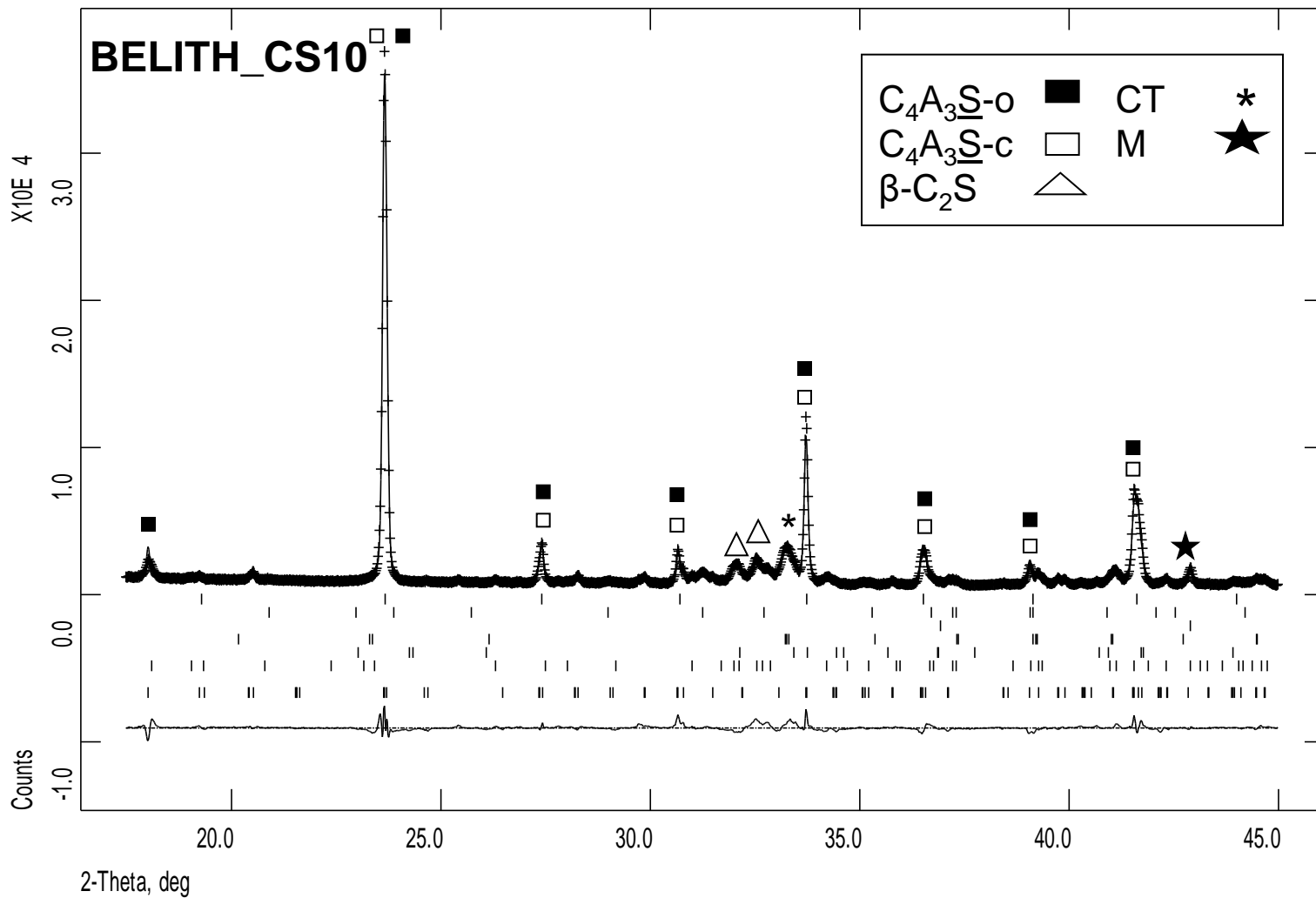


Figure 2

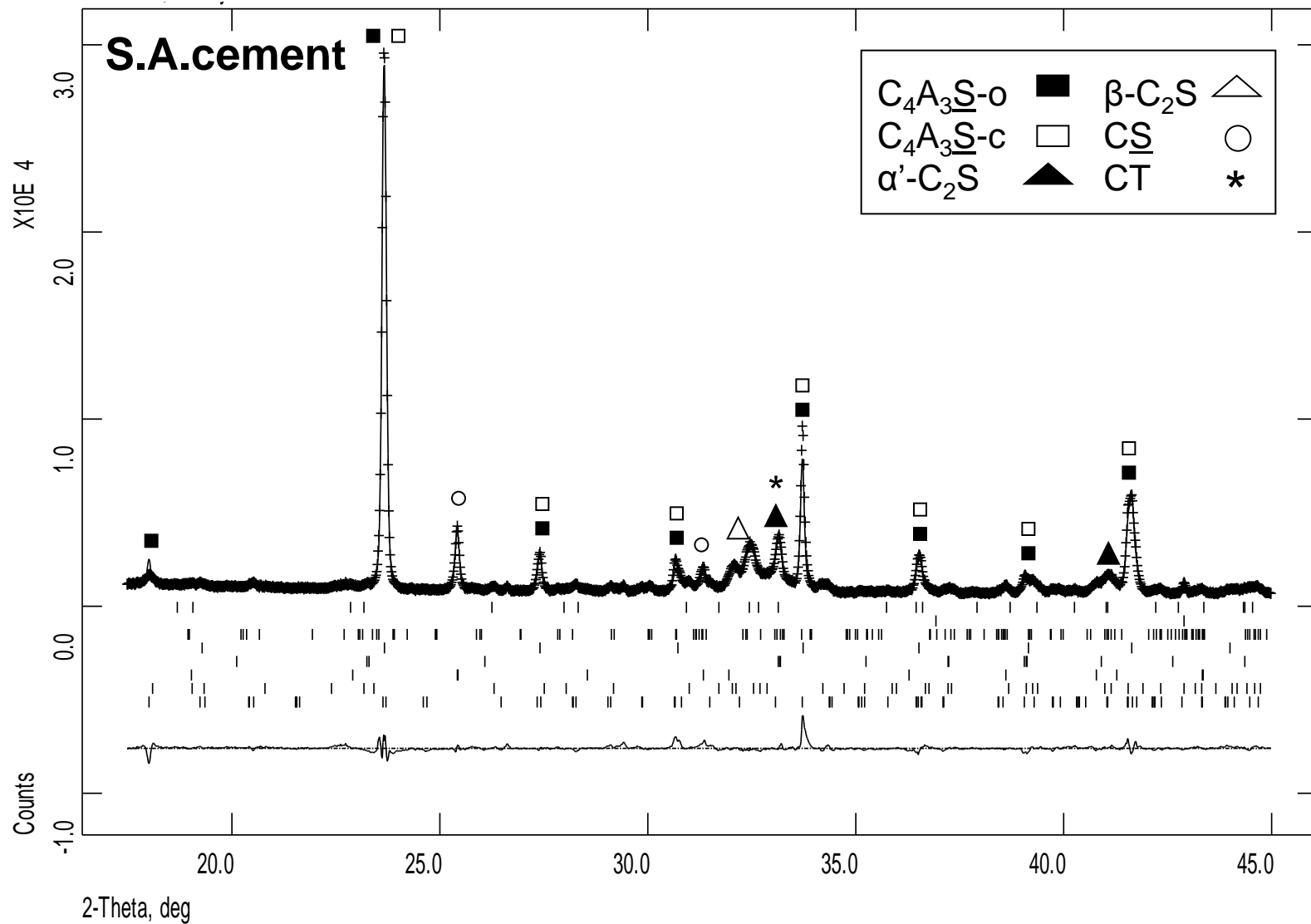


Figure 3

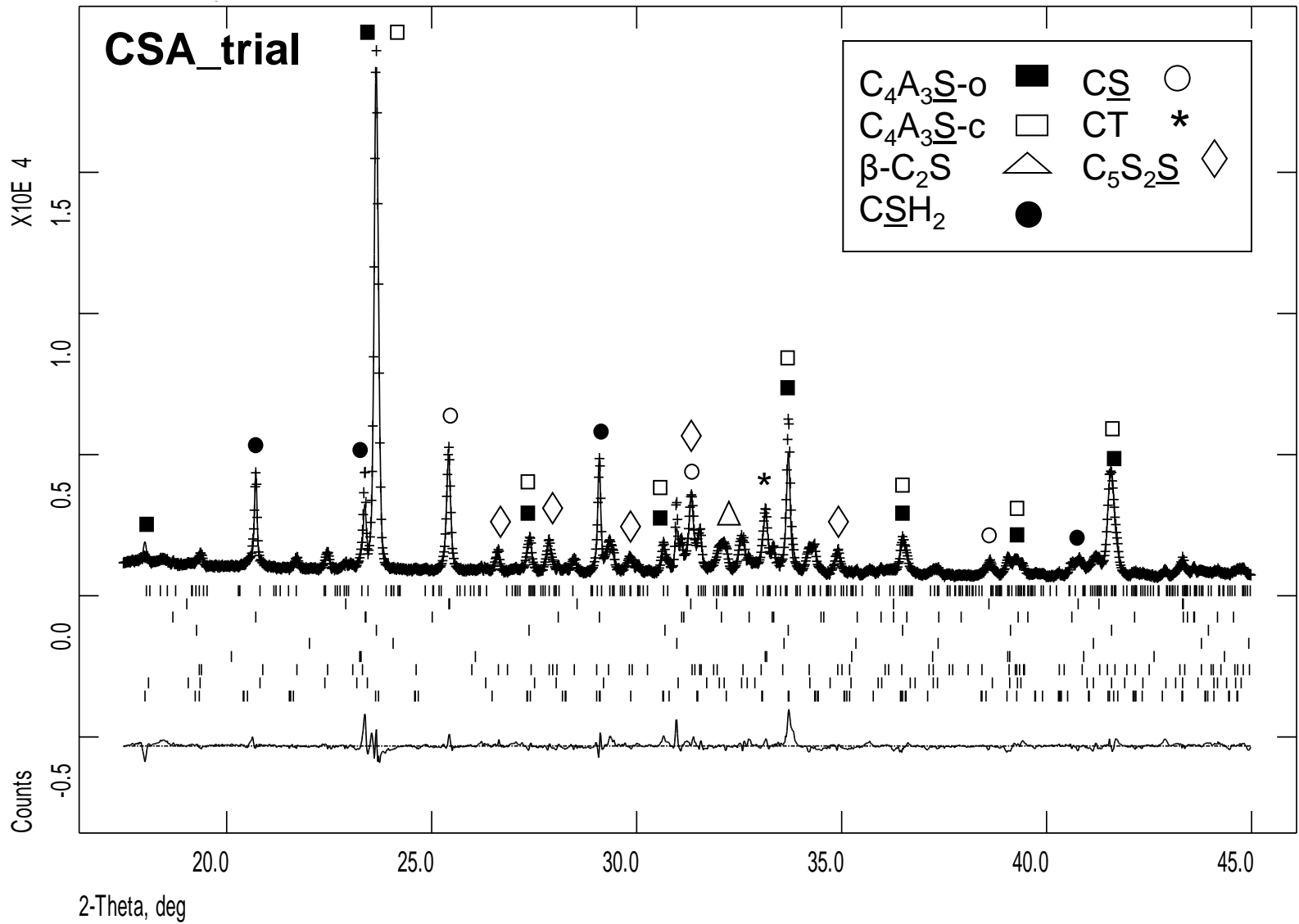


Figure 4

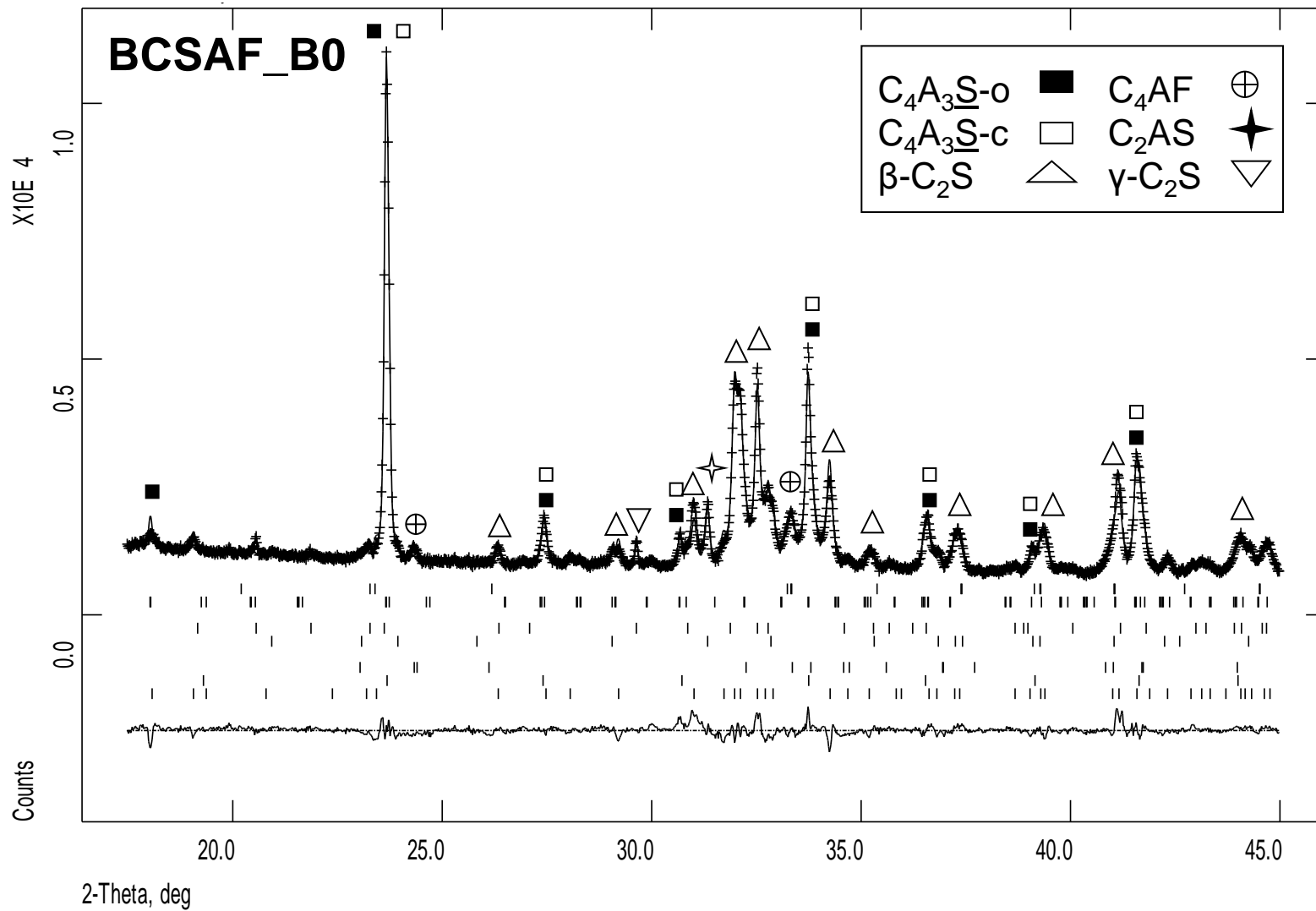


Figure 5

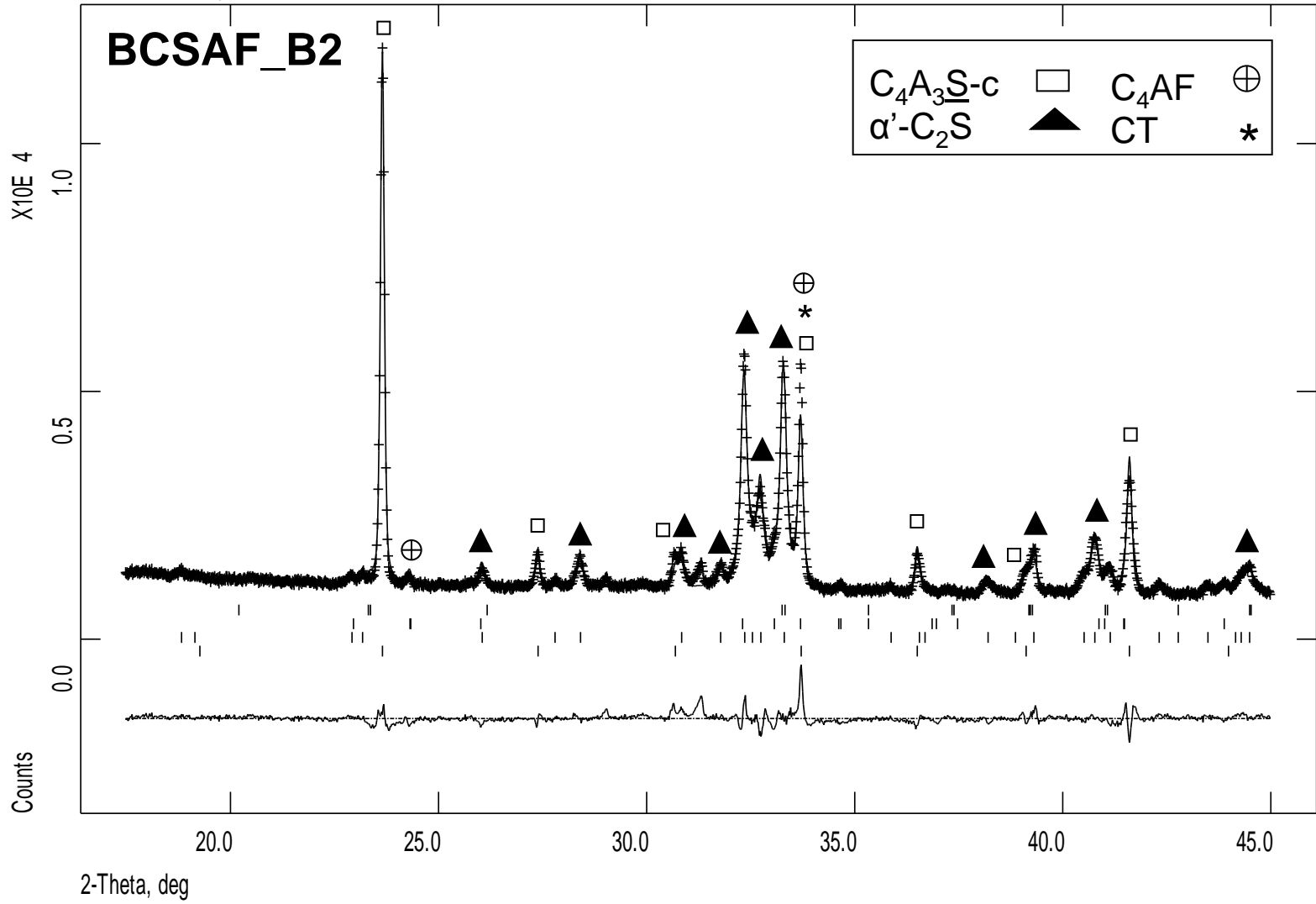


Figure 6

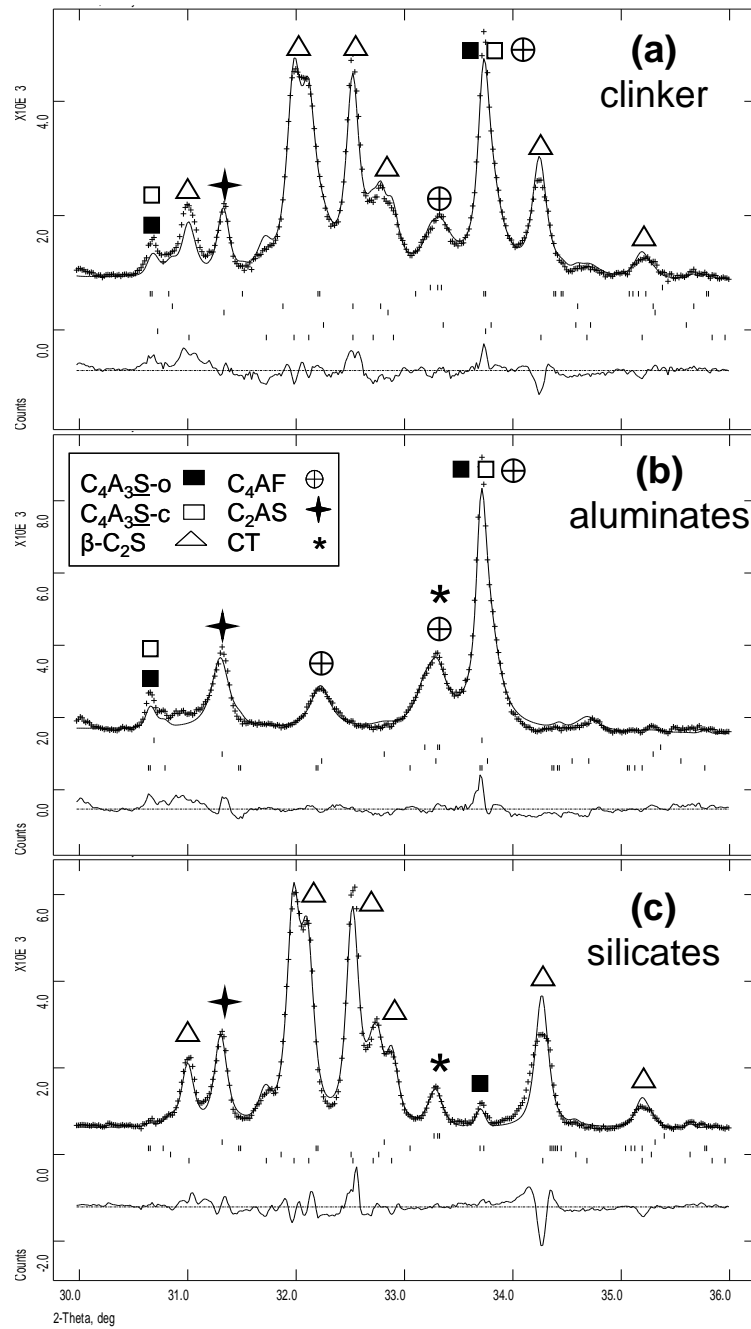


Figure 7

